Collapse and Rebound of a Laser-Induced Cavitation Bubble

I. Akhatov, A. Topolnikov, N. Vakhitova
Ufa Branch of the Russian Academy of Sciences, Ufa, Russia
O. Lindau, R. Mettin and W. Lauterborn
Universität Göttingen, Göttingen, Germany

Abstract

Single cavitation bubble luminescence (SCBL) induced by laser in contrast to single bubble sonoluminescence (SBSL) has no need in a sound field for a strong collapse and for light emission. The cavitation bubbles are produced by focused laser light and make the single strong collapse. As shown experimentally, the number of emitted photons from cavitation luminescence is much greater than it was observed in sonoluminescence due to the large bubble size during the final stage of collapse.

To describe the process of laser–induced bubble collapse a mathematical model is proposed, which is based upon the spherically–symmetric motion. The basic results of the numerical solution are presented for the bubbles with initial radii of about 1 mm. According to the observed results the minimum bubble radius in collapse is about 15 μm, and the mass decreases up to 5% of the initial value. The calculations show a good agreement with experimental measurements.

1. Introduction

The bubbles filled with gas or vapor can emit light when collapsing violently in a surrounded liquid upon strong excitation. A great interest in single, spherically collapsing bubbles in the last decade is associated with observation of single bubble sonoluminescence (SBSL), which is a light emission phenomenon of a stably oscillating bubble in a liquid irradiated by the periodical ultrasonic wave field (Gaitan et al., 1992; Barber et al., 1997). Although the duration of each light flash in sonoluminescence does not exceed 300 ps (Gompf et al., 1997) and occurs once a cycle, the periodical character of bubble motion makes the light visible to the unaided eye as the sum of many flashes.

Another method of single bubble investigation is provided by optic cavitation, when the transient cavities in the liquid are produced by strong laser pulses (Buzukov and Teslenko, 1971; Lauterborn, 1974). Single cavitation bubble luminescence (SCBL) in contrast to SBSL has no need in a sound field for a strong collapse and light emission. The laser–induced bubbles consist mainly of vapor, and their lifetime is estimated only a few rebounds. As compared to acoustically driven bubbles in SBSL they have larger size (about 1 mm at maximum and 10 μm in collapse) and produce light flash duration of a few nanoseconds (Baghdassarian et al., 1999). As shown experimentally (Ohl et al., 1999), the number of emitted photons from cavitation luminescence is much greater than it was observed in sonoluminescence.

In this paper some theoretical explanation for the dynamics of laser–induced cavitation bubble is proposed. A mathematical model of the spherically–symmetric motion of bubble is presented, which describes gas and liquid dynamics including compressibility, heat and mass transfer effects and diffusion both inside the bubble and in the liquid. Taking into account that nonequilibrium processes of evaporation and condensation must play a major role in bubble dynamics, we have used a detailed Hertz–Knudsen–Langmuir model to describe mass transfer through the bubble surface. A complicated equation of state of water in Mie–Grüneisen form is employed, that is valid for high compression and reasonable expansion of water.

On the base of the mathematical model had been constructed the numerical simulation of the problem was carried out for different maximum radii of laser–induced vapor bubble. The results showed a good agreement with experimental data on the minimum radius value and the maximum bubble radius after rebound. As obtained by calculations the small amount of noncondensable gas (about 1% of bubble mass) strongly influences the bubble dynamics.

2. The dynamics of vapor bubble

To model the problem we start from the instant where the bubble has reached its maximum radius. At this moment the temperature of the bubble is assumed to be equal to the surrounded liquid temperature, and the vapor pressure inside the bubble equals the saturation pressure at that temperature, which is much smaller than the liquid pressure. Because of the pressure jump the cavity must contract.

The entire gas–liquid region is divided into three zones (Nigmatulin et al., 2000a; Nigmatulin et al., 2000b): 1) gas–vapor zone ($0 \leq r \leq a(t)$), where $a(t)$ is the bubble radius, 2) "liquid drop" zone ($a(t) <$

$r \leq R(t)$), filled with compressible water, whose external radius $R(t)$ is about several radii in size and much smaller than the characteristic size of cuvette, and 3) weakly compressible liquid zone ($R(t) < r < \infty$) between "liquid drop" and the cuvette wall.

According to this scheme the radial velocity of the "liquid drop" wall $\dot{R}(t)$ is always small with respect to the speed of sound in water. This allow us to describe the behavior of $R(t)$ using generalized Rayleigh–Plesset equation without numerical calculations in zone 3).

In the absence of viscosity, diffusion and non–mechanical energy loss (due to radiation) the spherically–symmetric equations for the conservation of mass, momentum and energy (including heat conductivity term), which describe the vapor dynamics inside the bubble ($0 \leq r \leq a(t)$) and the compressible liquid for $a(t) < r \leq R(t)$, are the following:

$$\frac{\partial \rho}{\partial t} + \frac{1}{r^2}\frac{\partial}{\partial r}\left(\rho u r^2\right) = 0, \tag{1}$$

$$\frac{\partial}{\partial t}(\rho u) + \frac{1}{r^2}\frac{\partial}{\partial r}\left(\rho u^2 r^2\right) + \frac{\partial p}{\partial r} = 0, \tag{2}$$

$$\frac{\partial e}{\partial t} + \frac{1}{r^2}\frac{\partial}{\partial r}\left(u r^2 (e+p) - \lambda r^2 \frac{\partial T}{\partial r}\right) = 0. \tag{3}$$

Here ρ, u, p, T and $e = \rho\varepsilon + \rho u^2/2$ are the density, velocity, pressure, temperature and the total energy per unit volume respectively, ε is the internal energy per unit mass and λ is the heat conductivity coefficient (the indices l and v for water and vapor parameters are omitted for brevity).

In the present calculations the vapor inside the bubble is modeled as a hard core van der Waals gas:

$$p_v = \frac{\rho_v B_v T_v}{1 - b_1 \rho_v} - b_2 \rho_v^2, \quad \varepsilon_v = \frac{B_v T_v}{\gamma - 1} - b_2 \rho_v, \tag{4}$$

where $B_v = 458.9$ J/(kg·K), $\gamma = 1.3$, $b_1 = 1.694 \cdot 10^{-3}$ m^3/kg, $b_2 = 1708.6$ J·m^3/kg^2 are vapor parameters (Yasui, 1995).

The water around the bubble satisfies Mie–Grüneisen model, which can be written in the form:

$$p_l = p_c(\rho_l) + \Gamma(\rho_l) c_V \rho_l T_l, \quad \varepsilon_l = \varepsilon_c(\rho_l) + c_V T_l + \varepsilon_{l0}(T_l). \tag{5}$$

Here

$$p_c(\rho_l) = A\left(\frac{\rho_l}{\rho_{l0}}\right)^{2/3} \exp\left[b\left(1 - \left(\frac{\rho_l}{\rho_{l0}}\right)^{-1/3}\right)\right] - K\left(\frac{\rho_l}{\rho_{l0}}\right)^{4/3}, \tag{6}$$

$$\varepsilon_c(\rho_l) = \frac{3A}{\rho_{l0} b} \exp\left[b\left(1 - \left(\frac{\rho_l}{\rho_{l0}}\right)^{-1/3}\right)\right] - \frac{3K}{\rho_{l0}}\left(\frac{\rho_l}{\rho_{l0}}\right)^{1/3}, \tag{7}$$

where $A = 3.492 \cdot 10^8$ Pa, $K = 8.283 \cdot 10^8$ Pa, $b = 16.0558$, $c_V = 3270$ J/(kg·K), $\rho_{l0} = 998$ kg/m^3 are chosen to satisfy experimental data, and $\Gamma(\rho_l)$ is a Grüneisen coefficient, which is assumed to be a function of water density:

$$\Gamma(\rho_l) = 0.57 + \frac{0.95}{1 + (\rho_l/\rho_{l0} - 1.65)^2/0.12} - \frac{0.28}{1 + (\rho_l/\rho_{l0} - 1)^2/0.07}, \quad \rho_l \geq \rho_{l0},$$

$$\Gamma(\rho_l) = 0.24 + 1.9 \cdot 10^{-4}\rho_l + 0.07\exp\left[-0.004\left(\rho_l - \rho_{l0}\right)^2\right], \quad \rho_l < \rho_{l0}. \tag{8}$$

As we describe vapor and water by different equations of state we have to use a correction term $\varepsilon_{l0}(T_l)$ in Eq. (**??**) to match the internal energies on the saturation line ($p = p_S(T)$) (Nigmatulin, 1991):

$$\varepsilon_v(\rho_{vS}(T), T) - \varepsilon_l(\rho_{lS}(T), T) = l(T) + p_S(T)\left(\frac{1}{\rho_{lS}(T)} - \frac{1}{\rho_{vS}(T)}\right), \tag{9}$$

where $l(T)$ is the specific heat of vaporization. The approximation of $\varepsilon_{l0}(T_l)$ gives the formulae

$$\varepsilon_{l0}(T_l) = 0, \quad T \geq T_{cr},$$

$$\varepsilon_{l0}(T_l) = -1.207 \cdot 10^3 T + 7.793 \cdot 10^5, \quad T < T_{cr}, \tag{10}$$

where $T_{cr} = 647$ K is the critical value of water temperature.

To describe evaporation and condensation processes the following boundary condition for the temperature gradients at the bubble wall is used:

$$\lambda_l \left.\frac{\partial T_l}{\partial r}\right|_{r=a} - \lambda_v \left.\frac{\partial T_v}{\partial r}\right|_{r=a} = j_v l\left(p_v|_{r=a}\right), \tag{11}$$

Here

$$j_v = \frac{\alpha}{\sqrt{2\pi B_v}}\left(\frac{p_S(T_l|_{r=a})}{\sqrt{T_l|_{r=a}}} - \frac{\Gamma_V p_v|_{r=a}}{\sqrt{T_v|_{r=a}}}\right) \tag{12}$$

is the rate of phase transition from a unit surface according to the modified Hertz–Knudsen–Langmuir formula (Schrage, 1953).

There also exists the phase temperature jump on the boundary:

$$T_l|_{r=a} - T_v|_{r=a} = [T], \quad [T] = 0.45\frac{j_v T_S}{\sqrt{2B_v T_S}\rho_v|_{r=a}} \tag{13}$$

which is obtained from analysis of the transfer processes in a thin Knudsen layer of vapor (Labuntsov and Muratova, 1972).

Liquid and vapor velocities at the bubble surface and the bubble velocity $\dot{a}(t)$ differ due to phase transition according to the formula:

$$u_v|_{r=a} = \dot{a} - \frac{j_v}{\rho_v}, \quad u_l|_{r=a} = \dot{a} - \frac{j_v}{\rho_l}. \tag{14}$$

The pressure jump at $r = a$ is described by standard boundary condition

$$p_v|_{r=a} = p_l|_{r=a} + \frac{2\sigma}{a} + \frac{4\mu_l u_l|_{r=a}}{a} = p_l|_{r=a} + \frac{2\sigma}{a} + \frac{4\mu_l}{a}\left(\dot{a} - \frac{j_v}{\rho_l}\right). \tag{15}$$

Here σ and μ_l are the surface tension and dynamic viscosity of water.

The "liquid drop" external radius $R(t)$ is defined by a generalized Rayleigh–Plesset equation (Nigmatulin et al., 2000c)

$$\left(1 - \frac{\dot{R}}{C_l}\right)R\ddot{R} + \frac{3}{2}\left(1 - \frac{\dot{R}}{3C_l}\right)\dot{R}^2 = \left(1 + \frac{\dot{R}}{C_l}\right)\frac{p_l|_{r=R} - p_{l0}}{\rho_{l0}} + \frac{R}{\rho_{l0}C_l}\frac{d}{dt}\left(p_l|_{r=R} - p_{l0}\right), \tag{16}$$

where $C_l = 1500$ m/s is the speed of sound in water.

In the present calculations the heat conductivity coefficients for vapor and water λ_v and λ_l, liquid viscosity μ_l, surface tension coefficient σ and the saturated vapor pressure p_S are approximated from tabulated data as well as specific heat of vaporization l (Rivkin and Alexandrov, 1980).

To decrease the computational efforts the homobaric assumption for vapor and the model of incompressible liquid are introduced (Nigmatulin and Khabeev, 1974), when velocity of the bubble wall is much less than the sound speed in the vapor (in practice we use condition $|u_v|_{r=a}|/C_v \le M_{crit} = 0.3$). Such simplifications avoid us the numerical calculations of differential equations in the entire region $0 < r < R_t$ during the predominant time of bubble motion. The homobaric model of vapor dynamics is solved on the basis of a second order implicit scheme in time and space, and the Dorman–Prince method (Hairer et al., 1987) is applied to solve the generalized Rayleigh–Plesset equation. The system of partial differential equations (1)–(3) is realized by a first order Godunov scheme in mixed Eulerian–Lagrangian coordinates (Godunov et al., 1976).

The basic results of the numerical solution of dynamics of a laser–induced bubble with $a_{max} = 1$ mm are shown in Figs. 1–2. At the initial moment, when $a_0 = a_{max}$, the pressure inside the bubble equals the saturated vapor pressure $p_{v0} = p_S = 2330$ Pa at $T_{v0} = T_{l0} = 296$ K, which is much less than the liquid pressure $p_{l0} = 1$ bar=101325 Pa. The obtained difference between vapor and water pressures leads to the bubble collapse and vapor mass loss due to the condensation process on the bubble surface.

The radius and vapor mass dependencies on time are shown in Fig. 1. The system of partial differential equations (1)–(3) is solved here only in the high Mach region of solution between two dots, all the other time

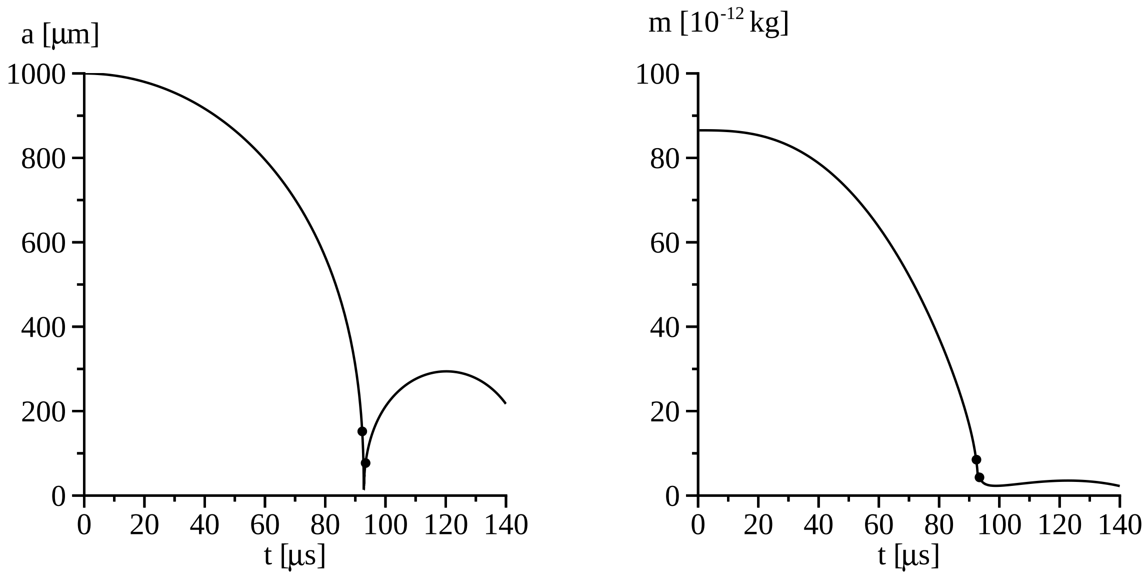

Figure 1: The vapor pressure and mass as functions of time. Dots show the time moments, at which the high–Mach period starts (first dot) and ends (second dot). Results are presented for $a_0 = 1$ mm, $\alpha = 0.075$.

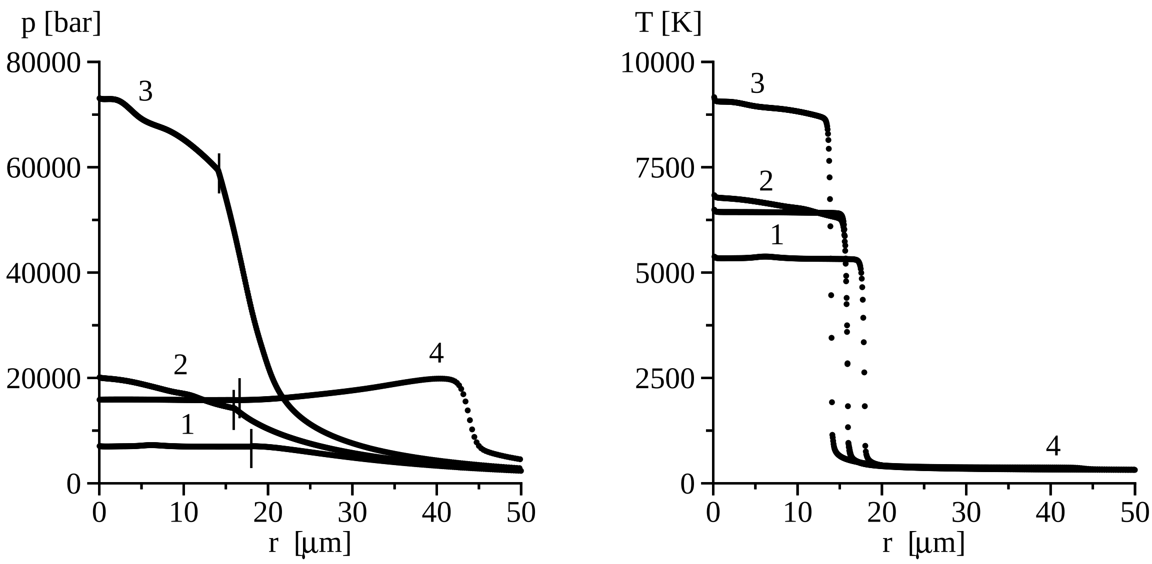

Figure 2: The pressure and temperature spatial distributions at four moments of time at collapse. Vertical lines mark the vapor bubble radius. Results are presented for $a_0 = 1$ mm, $\alpha = 0.075$.

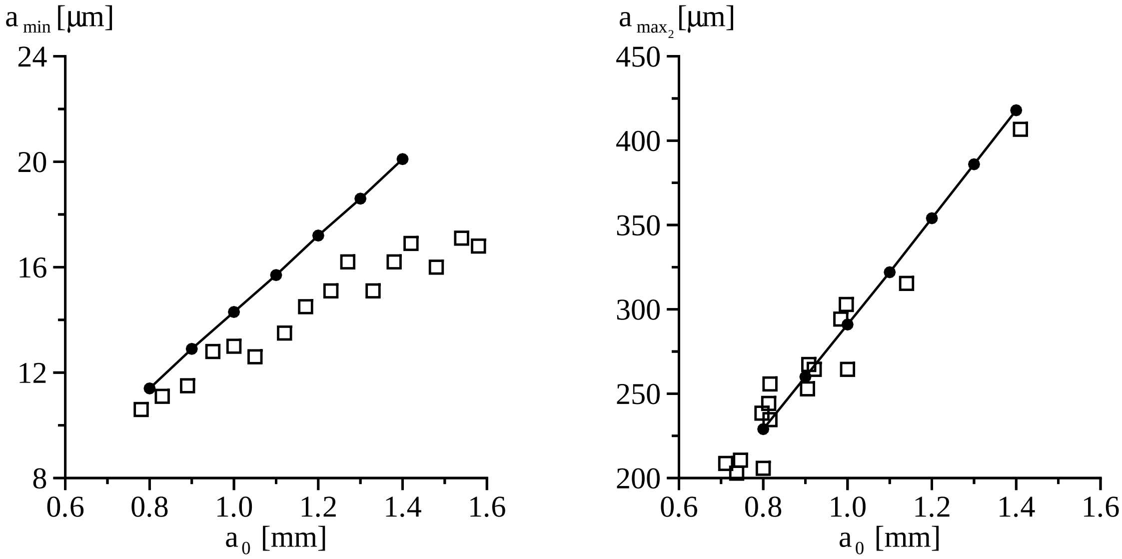

Figure 3: Comparison between experimental data symbols and numerical results (dotted line) on the minimum bubble radii at collapse and first after collapse maximum bubble radii for different initial bubble sizes.

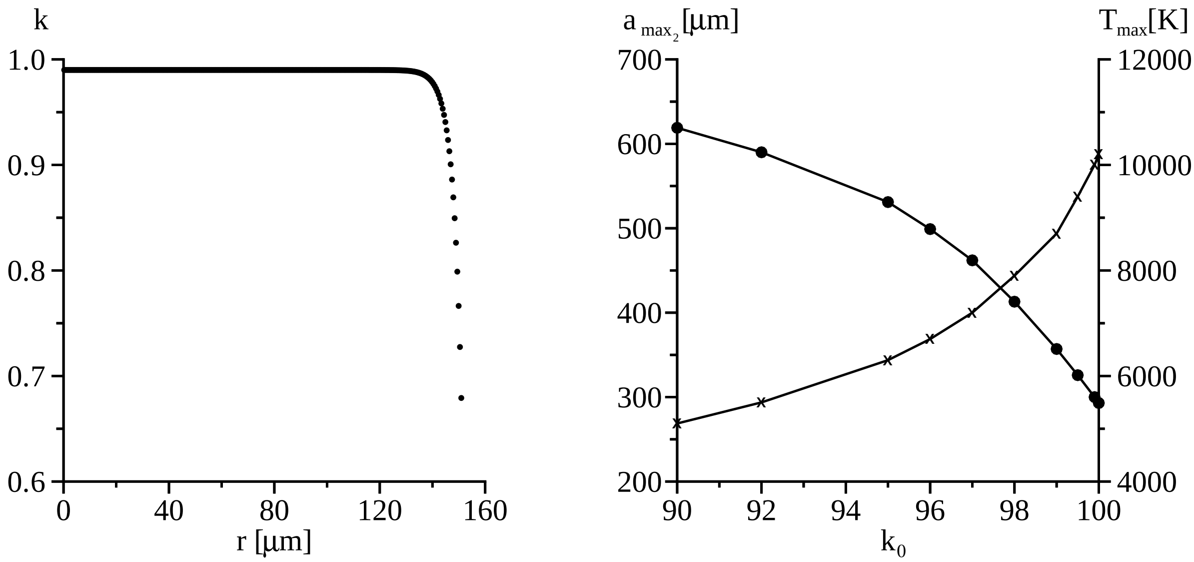

Figure 4: The typical vapor concentration distribution during the bubble compression stage (t=-529.58 ns before collapse). The first maximum bubble radius after collapse (dotted line) and the peak value of bubble temperature (dashed line with symbols) as functions of initial vapor concentration. Results are presented for $a_0 = 1$ mm, $\alpha = 0.075$.

we use the simplified homobaric model to describe vapor dynamics and incompressible liquid assumption for water (R_0 equals $1.5a_0$). The calculated minimum bubble radius is about 14 μm and at collapse the mass decreases down to 6% of the initial value. These results have been obtained for an accommodation coefficient $\alpha = 0.75$ in Eq. (12). Because of the contradictory data on the accommodation coefficients for water exist we use here α as an adjustable parameter to fit experimentally measured value of the maximum bubble radius after rebound a_{max_2}, and the other numerical simulations have been carried out with that same value of α.

The spatial distributions of pressure and temperature at around the time of collapse are displayed in Fig. 2. There are no shock waves observed inside the bubble during its maximum compression. The pressure profile is almost uniform and p_v reaches approximately 10^5 bar in the center, the corresponding temperature value does not exceed 10^4 K, which is quite enough to produce light (Hilgenfeldt et al., 1999). The collapsing bubble initiates a strong outgoing shock wave in the water ($t = t_4$).

Fig. 3 presents a comparison between experimental data (symbols, Ohl et al., 1999) and the numerical results (solid lines with dots) on the minimum bubble radius at the collapse (a_{min}) and the maximum radius of the first rebound (a_{max_2}) for different initial bubble sizes ($a_0 = a_{max}$). Despite of small systematic deviation for a_{min} the calculations agree well with the experimental results.

3. Gas–vapor bubble dynamics

The previous calculations has been done assuming that the bubble consists of vapor only. A real bubble, however, contains a small amount of noncondensable gas, which can be a product of duffision from the surrounded liquid, plasma recombination or chemical reactions. To estimate the influence of the gas presence inside the bubble we have to extend our mathematical model by introducing two component mixture as a gas phase.

In such a case the governing equations for the vapor–gas mixture dynamics at $0 \le r \le a(t)$ will be Eqs. (1)–(2) and the energy equation in the form

$$\frac{\partial e}{\partial t} + \frac{1}{r^2}\frac{\partial}{\partial r}\left(ur^2\left(e+p\right)\right) = \frac{1}{r^2}\frac{\partial}{\partial r}\left(\lambda r^2 \frac{\partial T}{\partial r}\right) + \frac{1}{r^2}\frac{\partial}{\partial r}\left(\rho r^2 D \frac{\partial k}{\partial r}\left(\varepsilon_v - \varepsilon_g\right)\right), \tag{17}$$

where k and D are the vapor mass concentration and the coefficient of binary diffusion.

To calculate k the diffusion equation is used:

$$\frac{\partial k}{\partial t} + u\frac{\partial k}{\partial r} = \frac{1}{\rho r^2}\frac{\partial}{\partial r}\left(\rho r^2 D \frac{\partial k}{\partial r}\right). \tag{18}$$

The vapor, gas and mixture parameters are related with the following accessory equations:

$$\rho_v = k\rho, \quad \rho_g = (1-k)\,\rho, \quad u = ku_v + (1-k)\,u_g, \quad p = p_v + p_g,$$

$$\varepsilon = k\varepsilon_v + (1-k)\varepsilon_g, \quad \rho_v\left(u - u_v\right) = -\rho_g\left(u - u_g\right) = \rho D\frac{\partial k}{\partial r}, \quad T = T_v = T_g, \tag{19}$$

where the subscript v denotes vapor and g – gas parameters. Gas–vapor mixtures parameters are written with no subscripts.

The noncondensable gas in the bubble is modeled as a van der Waals gas (**??**)–(**??**) with parameters of air (Yasui, 1995): $B_g = 284.75$ J/(kg·K), $\gamma_g = 1.4$, $b_{1g} = 1.294 \cdot 10^{-3}$ m^3/kg, $b_{2g} = 166.7$ J·m^3/kg^2. The coefficient of binary diffusion of vapor in the air is chosen to be function of temperature according to the formula (Grigoriev and Meilikhov, 1991)

$$D = 2.16 \cdot 10^{-5}\left(\frac{T}{273}\right)^{1.80}. \tag{20}$$

Let us assume that a small amount of gas is dissolved in the water around the bubble. The liquid dynamics will be still described by Eqs. (1)–(3), and the mass concentration of gas c is defined by

$$\frac{\partial c}{\partial t} + u_l\frac{\partial c}{\partial r} = \frac{1}{\rho_l r^2}\frac{\partial}{\partial r}\left(\rho_l r^2 D_l \frac{\partial c}{\partial r}\right). \tag{21}$$

The appearance of diffusion flux through the bubble surface changes the boundary conditions:

$$u|_{r=a} = \dot{a} - \frac{j_v + j_d}{\rho|_{r=a}}, \quad \rho D \left.\frac{\partial k}{\partial r}\right|_{r=a} = (1-k)j_v - kj_d, \tag{22}$$

$$c|_{r=a} = Hp_g|_{r=a}, \quad j_d = \rho_l D_l \left.\frac{\partial c}{\partial r}\right|_{r=a}. \tag{23}$$

Here D_l is the diffusion coefficient of gas in a water and H is Henry's law constant. We use the following parameter values: $D_l = 1.76 \cdot 10^{-9}$ m^2/s and $H = 1.481 \cdot 10^{-10}$ Pa^{-1} (Yasui, 1995).

The approximation of the gas mass in the bubble, which can be absorbed there by diffusion flux from the liquid during its first expansion, can be done if we consider the following problem:

$$\frac{\partial c}{\partial t} + \frac{a^2 \dot{a}}{r^2}\frac{\partial c}{\partial r} = \frac{D_l}{r^2}\frac{\partial}{\partial r}\left(r^2 \frac{\partial c}{\partial r}\right), \tag{24}$$

$$c|_{r=\infty} = c_\infty, \quad c|_{r=a(t)} = c_a(t). \tag{25}$$

The analytical solution of Eqs. (24)–(25) with the gas concentration presented in the form

$$c(r,t) = c_\infty + (c_a(t) - c_\infty)\exp\left(-\frac{r-a(t)}{\delta(t)}\right), \tag{26}$$

where $\delta = \sqrt{D_l \Delta t}$ is the effective thickness of the diffusion boundary layer, Δt is the characteristic time of expansion, gives the following upper estimation for the gas mass in the bubble:

$$m_g \approx 4\sqrt{2D_l \Delta t}\pi a_{max}^2 H p_{l0} \rho_{l0}. \tag{27}$$

Taking the characteristic values $D_l \approx 10^{-9}$ m^2/s, $\Delta t \approx 10^{-4}$ s, $a_{max} \approx 10^{-3}$ m and $H \approx 10^{-10}$ Pa we get the following estimation: $m_g \approx 5 \cdot 10^{-14}$ kg, that is three to four orders of magnitude less than the mass of the vapor at maximum bubble radius and does not influence its dynamics considerably.

The numerical investigations on the base on the two component gas phase model have been carried out with initial vapor concentration of 99% (1% of noncondensable gas). The other parameters were chosen the same as in the previous calculations for vapor bubble. The now observed minimum bubble radius is 16.5 μm, the maximum radius of rebound equals 360 μm and the total mass of gas–vapor mixture in collapse is about $8 \cdot 10^{-12}$ kg. Comparing these data with the results obtained for vapor bubble (14 μm, 280 μm and $5.5 \cdot 10^{-12}$ kg correspondingly) one can say that a small addition of noncondensable gas strongly influences the bubble dynamics.

To explain such the phenomena we consider the profile of vapor concentration during the stage of bubble compression. As shown in Fig. 4 there is a strongly uniform distribution of concentration inside the bubble: $k = 0.99$ near the center and $k \approx 0.65$ at the boundary. As a result of forming a gas shell at the bubble wall, the partial vapor pressure in this zone essentially decreases, condensation rate stops and a resulting greater final mass is found in the bubble in collapse. Fig. 4 also presents the calculated results with different initial gas concentration values for a_{max_2} and T_{max}. The increase of noncondensable gas amount from 0 up to 10% leads to a sharp growth of radius after rebound from 290 up to 620 μm and to a decrease of peak temperature value in the bubble from 10000 K to 5200 K.

4. Conclusions

A mathematical model for the spherically–symmetric motion of a laser–induced bubble is proposed, which includes gas and liquid compressibility, heat and mass transfer due to evaporation and condensation processes on the bubble wall. In common case the model accounts that the bubble consists of two components: vapor and noncondensable gas and a small amount of last one is dissolved in the liquid.

Numerical simulations of vapor bubble dynamics showed that the evaporation and condensation on the bubble surface play the essential role in the problem. The mass loss during the compression stage makes strong collapse and allows vapor to achieve high pressures and temperatures. Calculations with different initial radii obtained a good agreement with experimental data on the minimum radius and the maximum radius after rebound.

It is shown that the mass of noncondensable gas accumulated in the bubble during its expansion by diffusion flux is negligibly small to affect the dynamics of a vapor cavity (less than 0.05%). Calculations with gas–vapor mixture were carried out for about 1% initial gas concentration. As shown numerically such the amount greatly influences bubble dynamics, essentially decreasing the condensation process on its surface.

Acknowledgement
The authors thanks Prof. R. I. Nigmatulin and Dr. R. Kh. Bolotnova for useful discussions of the equations of state for water. The work was supported by Internationales Büro des BMBF (Contract RUS–133–1997), European Commission (INCO–Copernicus, Contract ERBIC15CT980141), Deutsche Forschungsgemeinschaft (LA 268/22–1), and Russian Ministry of Science and Technology.

References

Baghdassarian O., Tabbert B., Williams G. A., 1999. Luminescence characteristics of laser–induced bubbles in water. Phys. Rev. Lett. 82 (12), 2437–2440.

Barber B. P., Hiller R. A., Löfstedt R., Putterman S. J., Weninger K. R, 1997. Defining the unknowns of sonoluminescence. Phys. Reports 281, 65–143.

Buzukov A. A., Teslenko V. S., 1971. Sonoluminescence following focusing of laser radiation into a liquid. Soviet Phys. JTEP Lett. 14, 189–191.

Gaitan D. F., Crum L. A., Roy R. A., Church C. C., 1992. Sonoluminescence and bubble dynamics for a single, stable cavitation bubble. J. Acoust. Soc. Am. 91, 3166–3172.

Godunov S. K., Zabrodin A. V., Ivanov M. Ya., Kraiko A. N., Prokopov G. P., 1976. Numerical solution of gas dynamics multidimensional problems. Nauka, Moscow.

Gompf B., Günther R., Nick G., Pecha R., Eisenmenger W., 1997. Resolving sonoluminescence pulse width with time–correlated single photon counting. Phys. Rev. Lett. 79 (7), 1405–1408.

Grigoriev I. S., Meilikhov E. Z., 1991. Physical values. Energoatomizdat, Moscow.

Hairer E., Norsett S., Wanner G., 1987. Solving ordinary differential equations. I. Nostiff problems. New York.

Hilgenfeldt S., Grossmann S., Lohse D., 1999. Sonoluminescence light emission. Phys. Fluids 11, 1318–1330.

Labuntsov D. A., Muratova T. M., 1972. Heat and mass transfer. Minsk.

Lauterborn W., 1974. Kavitation durch Laserlicht. Acustica 31, 52–78.

Nigmatulin R. I., Khabeev N. S., 1974. Heat exchange between a gas bubble and a liquid. Fluid Dynamics 9, 759–764.

Nigmatulin R., 1991. Dynamics of multiphase media, Vol. 1, 2. Hemisphere, New York.

Nigmatulin R. I., Akhatov I. Sh., Vakhitova N. K., Topolnikov A. S., 2000. Bubble collapse and shock wave formation in sonoluminescence. AIP conference proceedings 524, 433–436.

Nigmatulin R. I., Akhatov I. Sh., Vakhitova N. K., Bolotnova R. Kh., Topolnikov A. S., Nasibullayeva E. Sh., Kalyakina O. L., Zakirov K. R., 2000. Mathematical modeling of a single bubble and multibubble dynamics in a liquid. Proc. Int. Conf. on Multiphase Systems, Ufa, Russia, 294–301.

Nigmatulin R. I., Akhatov I. Sh., Vakhitova N. K., Lahey R. T. Jr., 2000. On the forced oscillations of a small gas bubble in a spherical liquid–filled flask. J. Fluid Mech. 414, 47–73.

Ohl C.-D., Kurz T., Geisler R., Lindau O., Lauterborn W., 1999. Bubble dynamics, shock waves and sonoluminescence. Phil. Trans. R. Soc. Lond. A 357, 269–294.

Rivkin C. L., Alexandrov A. A., 1980. Thermodynamical properties of water and water vapor. Energiya, Moscow.

Schrage R. W., 1953. A theoretical study of interphase mass transfer. Columbia U. P., New York.

Yasui K., 1995. Effects of thermal conduction on bubble dynamics near the sonoluminescence threshold. J. Acoust. Soc. Am. 98 (5), 2772–2782.